PROBLEMS OF MECHATRONICS
ARMAMENT, AVIATION, SAFETY ENGINEERING

ISSN 2081-5891

1 (3), 2011, 7-24

Regarding the Influence of High Frequency Combustion Instabilities on Operation of Solid Rocket Motors*

Doru SAFTA, Titica VASILE, Ioan ION

Military Technical Academy
81-83 George Cosbuc Avenue, 050141 Bucharest, Romania

Abstract. High frequency combustion instabilities imply a major risk for the solid rocket motor's stable operation and they are directly linked to the response of the solid propellant to the pressure coupling. Our paper aims at defining a linearized one-dimensional flow study model of the solid propellant rocket motors' disturbed functioning analysis. Experimental researches were done with an adequate setup, built and improved in our lab, functioning on the basis of the nozzle throat intermittent modulating technique developed by ONERA researchers, able to evaluate the propellant response by the interpretation of the pressure oscillations damping in terms of propellant response.
Keywords: thermodynamics of rocket propulsion, unsteady solid propellant combustion, combustion instabilities, pressure-coupled response, rocket motor operation stability

1. INTRODUCTION

Combustion instability is a major concern in all propulsion and power generation systems. It is characterized by vibrations within the combustion chamber, generally measured as an oscillating pressure.

* Presented at 8th International Armament Conference on „Scientific Aspects of Armament and Safety Technology", Pułtusk, Poland, 6-8 October, 2010.

The paper's main task is to study the influence of high frequency of the oscillatory pressure on the solid rocket motor operation.

In this order, we are interested to obtain in the first stage, the influence of case average pressure level, in direct connection with the oscillation frequency level on the propellant response function. The pressure coupled response is the often referred parameter to describe combustion instability characteristics of a rocket propellant. This type of response is accepted to be an important function able to characterize the motor working stability, hence to express the motor working behavior.

An investigation of combustion instability in solid rocket motors was done in our labs considering the association of two principals: the disturbing of a subscale test motor by intermittent modulating of its nozzle throat and the interpretation of the induced pressure oscillations damping in terms of propellant response. Our investigation setup is similar with the experimental device *propulseur à éjection modulé – PEM* promoted by ONERA researchers [3, 4, 6] having as its main part a subscale test solid rocket motor. By this important component and the facility to explore high frequency motor operation the jet intermittent modulating technique brings certain advantages as an indirect investigation method for longitudinal instabilities [2, 3, 6].

Our theoretical researches were focused on defining an adequate study model for the solid rocket motors disturbed operation, analyzing mainly the propellant response function to the pressure coupling on the basis of the pressure – time evolution for various propellants. It's about an interdisciplinary research study in order to realize a better modeling of the rocket motors perturbed operation at high frequencies. The high frequency pressure oscillations including their alternative components provide the main information to evaluate the propellant response.

2. MATHEMATICAL MODEL

2.1. Assumptions and basic equations

In order to make the analysis easier to be implemented and amenable to solution, many simplifying assumptions are considered in our presentation, but the essential features of combustion – flow process is retained in our study model.

The working fluid is considered as a mixture of gases assumed to be homocompositional as well as thermally and calorically perfect. The flow will be assumed to be non-heating-conducting. Our study is based on the general form of conservation equations [2-4], for one – dimensional motion of gases in the grain core, with cross-area variable along the motor case:

Conservation of Mass:

$$\frac{\partial}{\partial t}(\rho A)+\frac{\partial}{\partial x}(\rho v A)=\rho_p u_b \frac{P_b}{\cos\theta} \tag{1}$$

Conservation of Momentum:

$$\frac{\partial}{\partial t}(\rho v A)+\frac{\partial}{\partial x}\left[\left(p+\rho v^2\right)A\right]=pP_p tg\,\theta \tag{2}$$

Conservation of Energy:

$$\frac{\partial}{\partial t}(\rho A H_i)+\frac{\partial}{\partial x}(\rho v A H_i)=A\frac{\partial p}{\partial t}+\rho_p u_b H_p \frac{P_b}{\cos\theta} \tag{3}$$

Equation of State: $$p=\rho RT \tag{4}$$

Although eqs. (1)-(4) are enough to determine the flow state, transport equations for certain other thermodynamic variables will also prove useful. In particular, we have:

Equation for the Entropy:

$$\frac{\partial S}{\partial t}+v\frac{\partial S}{\partial x}=\frac{2\,\gamma\rho_p u_b}{\rho a^2 r\cos\theta}\left[(\gamma-1)\left(\frac{v^2}{2}+H_p-a^2\right)\right] \tag{5}$$

The mathematical model took into account the local propellant burning rate, $\vec{u}_b$ (absolute propellant wall velocity), the burning products emission velocity from burning surface, $\vec{u}_g$, [3] (Fig. 1) and of the local burning perimeter P_b, (Fig. 2):

$$u_g=u_b\left(\frac{\rho_p}{\rho}-1\right),\qquad P_b=\frac{\partial A_b}{\partial x}\cos\theta=\frac{1}{u_b}\frac{\partial A}{\partial t}\cos\theta \tag{6}$$

The total enthalpy of gas in every slide of the grain core, H_i and H_p, the total enthalpy of propellant burning products are expressed as

$$H_i=h_i+\frac{v^2}{2}=\frac{\gamma}{\gamma-1}\frac{p}{\rho},\qquad H_p=h_p+\frac{u_g^2}{2} \tag{7}$$

The grain geometry (Fig. 2) is expressed by the following non-dimensional parameters:

$$b_1=\frac{r_1}{r_2},\quad b_2=\frac{L}{2r_2},\quad X=\frac{e}{r_2}\le 1-b_1,\quad Y=\frac{A_b}{\pi r_2^2}$$

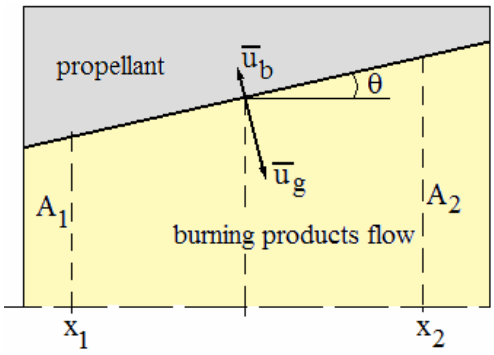

Fig. 1. The local burning rate and the products emission velocity vectors at the burning surface level

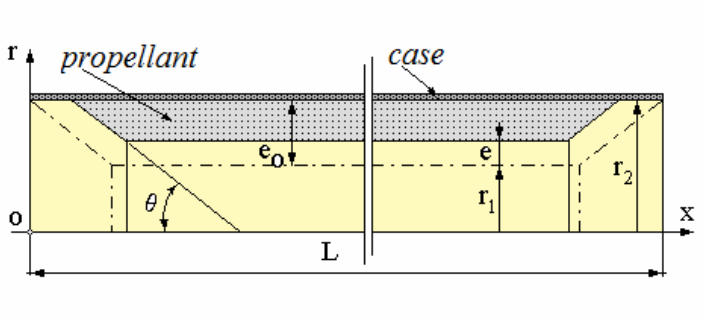

Fig. 2. Schematic of propellant grain geometry

2.2. Unsteady model

The fundamental equations (1)-(5) are nonlinear. However, a linearization process is possible using the method of regular perturbations. In this process, the internal flowfield is separated into two components, a steady part and an unsteady or oscillatory part.

The unsteady burning and flow processes generally provide an oscillatory pressure in the motor chamber. Our study cases pointed out the presence of small pressure oscillations around the case average pressure ($\Delta p_{\max} \le 0{,}5\,bar$, $p'/\overline{p} << 1$). Hence, the acoustic linear analysis can be applied and the pressure oscillations can be considered as harmonic oscillations.

Since the time – dependent part is oscillatory, then each of the independent variables [4, 5] can be written as

$$F(x,t) = \underbrace{F^{(0)}(x)}_{steady} + \underbrace{F^{(1)}(x,t)}_{time-dependent} \cong \overline{F} + \varepsilon F' = \overline{F} + \varepsilon\,\mathrm{Re}\left(\tilde{F}(x)e^{-\alpha t}e^{i\omega t}\right)$$

We introduce the following non-dimensional variables:

$$\delta' = \frac{\rho'}{\overline{\rho}}, \varphi' = \frac{p'}{\overline{p}}, \nu' = \frac{v'}{\overline{a}}, \mu' = \frac{m'}{\overline{m}} = \frac{u_b'}{\overline{u}_b}, \tau_p' = \frac{H_p'}{\overline{H}_p} = \frac{T_b'}{\overline{T}_b}, x^* = \frac{x}{L}, r^* = \frac{r}{r_2} \tag{8}$$

where: $m = 2\,\rho_p\,u_b/(r\cos\theta)$.

Defining each unsteady component $F' = \mathrm{Re}(\tilde{F}\,e^{i\Omega\tau}) = \tilde{F}\cos(\Omega\tau)$, where:

$\tilde{F}$ – amplitude of unsteady component variation,

$\tau = \overline{a}_0\,t/L$ – normalized time,

$\Omega = \frac{L}{\overline{a}_0}(2\pi\,f + i\,\alpha)$ – normalized pulsation in complex form, in which the frequency *f* and damping α parameter appear.

By adequate transformations of eqs. (1-3, 5) we obtain:

$$i\Omega\tilde{\nu} + \frac{1}{\gamma}\frac{d\tilde{\varphi}}{dx^*} = -\overline{M}_L\left[\frac{2}{r^*}\frac{d(M_1 r^*)}{dx^*}\tilde{\nu} + M_1\frac{d\tilde{\nu}}{dx^*}\right] \tag{9}$$

$$i\Omega\tilde{\varphi} + \gamma\frac{1}{r^{*2}}\frac{dr^{*2}}{dx^*}\tilde{\nu} + \gamma\frac{\partial\tilde{\nu}}{\partial x^*} = \overline{M}_L\left[\frac{\gamma}{r^{*2}}\frac{d(M_1 r^{*2})}{dx^*}(\tilde{\mu} + \tilde{\tau}_p - \tilde{\varphi}) - M_1\frac{\partial\tilde{\varphi}}{\partial x^*}\right] \tag{10}$$

$$i\Omega\tilde{S} = \overline{M}_L\left\{\frac{\gamma}{r^{*2}}\frac{d(M_1 r^{*2})}{dx^*}\left[\tilde{\tau}_p + (\gamma-1)\tilde{\varphi} - \gamma\tilde{S}\right] - M_1\frac{\partial\tilde{S}}{\partial x^*}\right\} \tag{11}$$

The solutions of this system can be expressed in the following form:

$$\begin{aligned} \tilde{\varphi} &= \tilde{\varphi}_0 + \overline{M}_L\tilde{\varphi}_1 + ... & \tilde{\nu} &= \tilde{\nu}_0 + \overline{M}_L\tilde{\nu}_1 + ... \\ \tilde{S} &= \tilde{S}_0 + \overline{M}_L\tilde{S}_1 + ... & \Omega &= \Omega_0 + \overline{M}_L\Omega_1 + ... \end{aligned} \tag{12}$$

where $\overline{M}_L = (\overline{v}/\overline{a})_L$ is the perturbation parameter.

According to the perturbations method, the eqs. (9)-(11) become:

– *order* "1":

$$i\Omega_0\tilde{\nu}_0 + \frac{1}{\gamma}\frac{d\tilde{\varphi}_0}{dx^*} = 0 \tag{13}$$

$$i\Omega_0\tilde{\varphi}_0 + \frac{\gamma}{r^{*2}}\frac{dr^{*2}}{dx^*}\tilde{\nu}_0 + \gamma\frac{d\tilde{\nu}_0}{dx^*} = 0 \tag{14}$$

$$\tilde{S}_0 = 0 \tag{15}$$

– order " $\overline{M}_L$ *":*

$$i\Omega_0\tilde{v}_1+\frac{1}{\gamma}\frac{d\tilde{\varphi}_1}{dx^*}=-\left[i\Omega_1+\frac{2}{r^*}\frac{d(M_1r^*)}{dx^*}\right]\tilde{v}_0-M_1\frac{d\tilde{v}_0}{dx^*} \tag{16}$$

$$\begin{aligned} &i\Omega_0\tilde{\varphi}_1+\frac{\gamma}{r^{*2}}\frac{dr^{*2}}{dx^*}\tilde{v}_1+\gamma\frac{\partial\tilde{v}_1}{\partial x^*}= \\ &\left[\frac{\gamma}{\tilde{\varphi}\,r^{*2}}\frac{d(M_1r^{*2})}{dx^*}(\tilde{\mu}+\tilde{\tau}_p-\tilde{\varphi})-i\Omega_1\right]\tilde{\varphi}_0-M_1\frac{\partial\tilde{\varphi}_0}{\partial x^*} \end{aligned} \tag{17}$$

$$i\Omega_0\tilde{S}_1=\left(\frac{\tilde{\tau}_p}{\tilde{\varphi}}+\gamma-1\right)\frac{\gamma}{r^{*2}}\frac{d(M_1r^{*2})}{dx^*}\tilde{\varphi}_0 \tag{18}$$

The boundary conditions are:

$$x^*=0:\quad \bullet\ \tilde{\varphi}_0=1,\ \tilde{\varphi}_1=0,\bullet\bullet\ \tilde{v}_0=0,\ \tilde{v}_1=0, \tag{19}$$

$$\tilde{\varphi}=\tilde{\varphi}_0=1,\varphi'=\mathrm{Re}\left(\tilde{\varphi}e^{i\Omega\tau}\right)=\cos[(\Omega_0+\overline{M}_L\Omega_1)\tau]$$

$$\tilde{v}=\tilde{v}_0+\overline{M}_L\tilde{v}_1=0,v'=\mathrm{Re}\left(\tilde{v}e^{i\Omega\tau}\right)=0$$

$x^*=1$: unsteady flow continuity condition at the nozzle entrance:

$$\tilde{v}=\overline{M}_L(v_L\,\tilde{\varphi}+w_L\,\tilde{S}),$$

v_L, w_L – normalized complex [4] coefficients/ nozzle admittance and coadmittance, thus:

$$\bullet\ \tilde{v}_0=0, \tag{20a}$$

$$\bullet\bullet\ \tilde{v}_1=v_L\,\tilde{\varphi}_0,\quad v_L \text{ computed for } \Omega_0. \tag{20b}$$

The *order "1" solution* is provided by eqs. (13) and (14) with boundary conditions (19) and (20a). We can obtain $\tilde{v}_0$ depending on $\tilde{\varphi}_0$ and Ω_0 [4, 5], and from eq. (14) we can write an unique differential eq. in $\tilde{\varphi}_0$. The normalized pulsation Ω_0 can be computed based on a transcendent eq. built in this stage. As the first evaluation of this parameter, $\Omega_0^{(0)}$, we have:

$$\Omega_0^{(0)}=2(X-1+a)\sin\left(\frac{k\pi(1-a)}{b\cos\alpha}\right)+k\pi \tag{21}$$

The eqs. (16) and (17) with boundary conditions (19) and (20b) provide the *solution of "* $\overline{M}_L$ *"order.*

In this case we can express $\tilde{v}_1$ depending on $\tilde{\varphi}_0$ and $\tilde{\varphi}_1$ – and an unique differential eq. in $\tilde{\varphi}_1$. The pulsation Ω_1 can be computed as solution of the following eq.:

$$2i\Omega_1 \mathrm{I}_1 = \gamma\left(\frac{\tilde{\mu}+\tilde{\tau}_p}{\tilde{\varphi}} - \frac{\gamma-1}{\gamma}\right)\mathrm{I}_2 - I_3 - (1+\gamma v_L) \tag{22}$$

where:

$$\left.\begin{aligned} I_1 &= \int_0^1 r^{*2}\,\tilde{\varphi}_0^2\,dx^*\,,\; I_2 = \int_0^1 \frac{d\left(M_1 r^{*2}\right)}{dx^*}\tilde{\varphi}_0^2\,dx^* \\ I_3 &= \int_0^1 \frac{d\left(M_1 r^{*2}\right)}{dx^*}\left(\frac{1}{\Omega_0}\frac{d\tilde{\varphi}_0}{dx^*}\right)^2 dx^* \end{aligned}\right\} \tag{23}$$

Analyzing these integrals we can identify a physical significance: I_1 *is proportional with chamber acoustic energy*, I_2 expresses *the interdependence/ coupling between the pressure oscillations and the combustion phenomenon*, I_3 shows *the acoustic energy spent to get an axial unsteady velocity of burning products – "flow turning" losses*. The last term of eq. (22) expresses the *acoustic energy losses in the nozzle*.

Considering the steady-state conditions, the eqs. system solutions may take the form:

$$\begin{aligned} \overline{p}^* &= P_0(x^*) + \overline{M}_L P_1(x^*) + \overline{M}_L^2 P_2(x^*) + ... \\ \overline{M} &= \overline{M}_L M_1(x^*) + \overline{M}_L^2 M_2(x^*) + ... \end{aligned} \tag{24}$$

with the following boundary conditions:

$$P_0(0)=1,\, P_1(0)=0,\, P_2(0)=0,..\; M_1(0)=0,\, M_2(0)=0,..\; M_1(1)=1,\, M_2(1)=0$$

The variation of the chamber static pressure $\overline{p}$, and the evolution of Mach number $\overline{M}$ in the grain core for various X parameter values (implicitly its time variation) can be obtained by integrating the system:

$$\begin{aligned} &\frac{d}{dx^*}\left(\overline{p}^*\,\overline{M}\,\sqrt{1+\frac{\gamma-1}{2}\overline{M}^2}\right) = \frac{4\,\rho_p\, b\,\overline{u}_b}{\overline{\rho}\,\overline{a}_0\, r_s^*\cos\theta} + \\ &-\overline{p}^*\,\overline{M}\,\frac{1}{(r_s^*)^2}\frac{d(r_s^*)^2}{dx^*}\sqrt{1+\frac{\gamma-1}{2}\overline{M}^2} \end{aligned} \tag{25}$$

$$\frac{d}{dx^*}\left[\bar{p}^*\left(1+\gamma \overline{M}^2\right)\right]=-\gamma\,\bar{p}^*\overline{M}^2\frac{1}{(r_s^*)^2}\frac{d(r_s^*)^2}{dx^*} \tag{26}$$

where $x^*=\frac{x}{L}$, $r_s^*=\frac{r}{L}$, $\bar{p}^*=\frac{\bar{p}}{\bar{p}_0}$.

According to this model, the variables *p* and *v* can be computed as functions of time:

$$\begin{aligned} p &= \bar{p}\,(1+\varepsilon\,\varphi') = \bar{p}_0[\mathrm{P}_0(\mathrm{x}^*)+ \\ &+ \overline{\mathrm{M}}_L\mathrm{P}_1(\mathrm{x}^*)]\{1+\varepsilon\,\mathrm{Re}[(\tilde{\varphi}_0+\overline{M}_L\tilde{\varphi}_1)e^{i(\Omega_0+\overline{M}_L\Omega_1)\tau}]\} \end{aligned} \tag{27}$$

$$v=\bar{v}+\varepsilon\,\bar{a}\,v'=\bar{a}\,\overline{M}_L M_1(x^*)+\varepsilon\,\bar{a}\,\mathrm{Re}[(\tilde{v}_0+\overline{M}_L\tilde{v}_1)e^{i(\Omega_0+\overline{M}_L\Omega_1)\tau}] \tag{28}$$

2.3. Propellant response to pressure coupling

In order to evaluate the propellant response it is necessary to know its dependence on the *oscillations amplitude and frequency, the nature of flow oscillations, on average pressure and the propellant composition* [1, 2].

In the case of a *motor working operation* as a *harmonic* one and assuming the propellant response is dependent of steady pressure and pulsation and taking into account only *the pressure coupling* and neglecting, the admittance corrections, we can write [2, 4, 5, 6]:

$R_{up}=\frac{\tilde{\mu}}{\tilde{\varphi}}=\frac{\tilde{u}_b/\bar{u}_b}{\tilde{p}/\bar{p}}$, response in burning rate to the pressure coupling,

$R_{Tp}=\frac{\tilde{\tau}_p}{\tilde{\varphi}}=\frac{\tilde{T}_b/\bar{T}_b}{\tilde{p}/\bar{p}}$, response in burning temperature to the pressure coupling. Thus:

$$R_p=R_{pc}=R_{up}+R_{Tp}=\frac{\tilde{\mu}+\tilde{\tau}_p}{\tilde{\varphi}} \tag{29}$$

is the propellant response in combustion to the rocket motor pressure coupling, named the linear propellant response. Taking into account the normalized pulsation, Ω, [4, 6, 7],

$$\Omega=\frac{L}{\bar{a}_0}(2\pi\,f+i\alpha)\cong\Omega_0+\overline{M}_L\Omega_1\Rightarrow i\Omega_1=-\frac{\alpha\,L}{\bar{a}_0\,\overline{M}_L}+\frac{i}{\overline{M}_L}\left(\frac{2\pi\,f\,L}{\bar{a}_0}-\Omega_0\right)$$

the real part and the imaginary one of the combustion response R_c will be:

$$\left.\begin{aligned} R_p^{(r)} &= \frac{\gamma-1}{\gamma}+\frac{1+\gamma\nu_L^{(r)}+I_3-\dfrac{2\alpha L}{\bar{a}_0\,\overline{M}_L}I_1}{\gamma I_2} \\ R_p^{(i)} &= \frac{\gamma\nu_L^{(i)}+\dfrac{2}{\overline{M}_L}I_1\left(\dfrac{2\pi f L}{\bar{a}_0}-\Omega_0\right)}{\gamma I_2} \end{aligned}\right\} \qquad (30)$$

2.4. Experimental setup

Experimental research was performed with an adequate experimental setup, built in our lab on the basis of the nozzle throat modulating device developed by ONERA researchers [2, 3, 5], able to evaluate the propellant response by the interpretation of the damping of pressure oscillations in terms of propellant response.

The perturbed working simulation device, in the frame of jet intermittent modulating techniques, offers many investigation opportunities [3, 4, 5, 6]. It is equipped with a special "*teeth wheel*" with 3 modulating teeth on a small wheel sector which spins at a given speed (depending on the studied range of frequencies) in a cross – section near the nozzle throat.

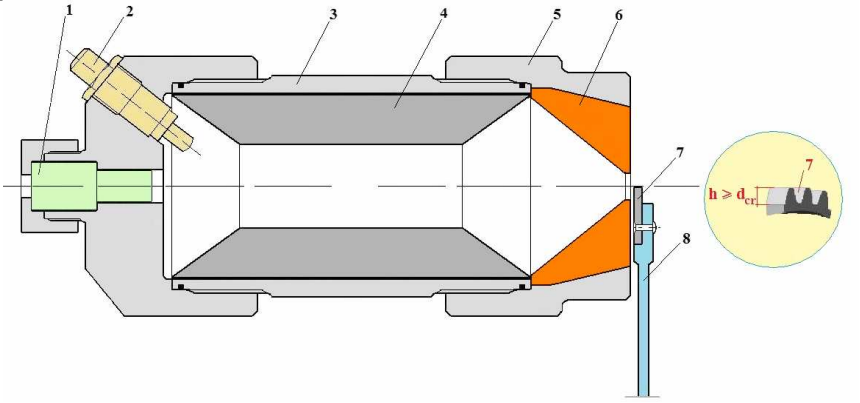

Fig. 3. Sketch of subscale test motor with modulating device:
1 – dynamic quartz piezoelectric sensor, 2 – igniter, 3 – chamber wall, 4 – propellant grain, 5 – aft end cover, 6 – nozzle, 7 – modulating teeth, 8 – modulating wheel

This autonomic setup measures by a dynamic quartz piezoelectric sensor the chamber pressure and records these data, for various grain shapes, and has multiple analyzing possibilities depending on time and frequency (Fig. 3).

The disturbing intensity is determined by the ratio of nozzle throat obturation and also by the position of the wheel plane as to the nozzle throat. Although this device is not really a continuous pulsator, this method could be used to drive selected frequencies during an experiment and numerous pulses could be obtained in a single test.

In our experiments with a non-metalized composite propellant the teeth wheel 7 (Fig. 3) was used to modulate the throat area at frequencies up to 7 kHz on each revolution. After the pass of the third tooth, the combustor gets into a natural damping process for the remaining part of the revolution time. The teeth sector during each pass operates obstructing 50% of the nozzle throat.

3. RESULTS AND CONCLUSIONS

In the frame of the developed model, the variations of unsteady pressure and flow velocity amplitude ($\tilde{\varphi}_0$, $\tilde{v}_0$), for longitudinal oscillation mode (k = 1), can be easily evaluated. Thus, one observes the parameter variation of $\tilde{\varphi}_0(x^*)$ is very appropriate of cos (πx^*), (Fig. 4). The flow velocity amplitude reaches maximum at the middle of the chamber and this parameter at the beginning of the burning is greater by about 30% than its value at the end of motor operation. We can assert, on the basis of the theoretical model, that the real part of propellant response – $R_p^{(r)}$, is a function of the *oscillation damping*, *acoustic energy* in the motor chamber and *various losses in the burning chamber*. The imaginary part of propellant response – $R_p^{(i)}$, mainly depends on the *normalized pulsation*, on the *burning chamber gas column* and on the pressure oscillations *frequency*.

The computing procedure of the propellant response evaluation model basically demands 3 types of data:

a) combustion products characteristics (thermodynamical calculus);

b) dimensions of the grain, case and nozzle;

c) experimental results – the average pressure, burned thickness, frequency and damping oscillations as time functions.

Applying our model, the main steps of computing procedure are:

- calculus of perturbation parameter $\overline{M}_L$ based on the rate (A_L / A_{cr}), [5];
- iterative calculus of normalized pulsation Ω_0, [4, 5], (first evaluation (21), Fig. 5);
- determining of the integrals I_1, I_2, I_3 and of $v_L^{(r)}$, $v_L^{(i)}$, [4-6];
- calculus of the global response in combustion R_p, eq. (30), using the experimental data obtained by jet intermittent modulating techniques.

Regarding the evaluation of the integrals I_1, I_2, I_3, for the considered grain shape, we can use a suitable analytical formula. Thus, Figure 6 depicts the variations of these integrals depending on the relative burning grain thickness for the first oscillation mode.

It's important to highlight that the grain core flow unsteady velocity calculus, eq. (28), demands to know $\overline{v}$, or $\overline{M}$ parameter, and for this reason the $M_1(x^*)$ evolution was computed by numerical integration, corresponding to $t \in \{0,\ (1/5)t_b,\ (2/5)t_b,\ (3/5)t_b,\ (4/5)t_b,\ t_b\}$, (Fig. 7).

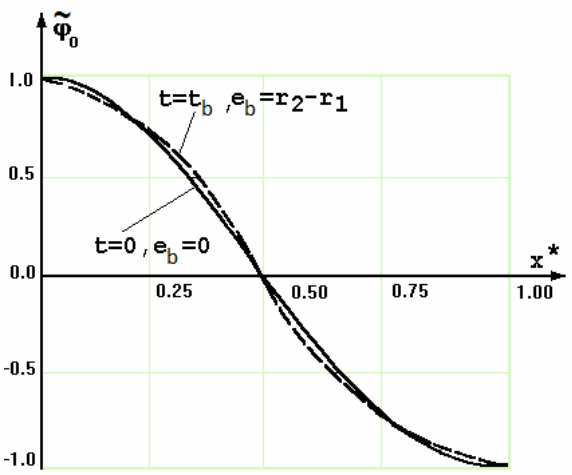

Fig. 4. Unsteady pressure amplitude $\tilde{\varphi}_0$ vs. non-dimensional length x*

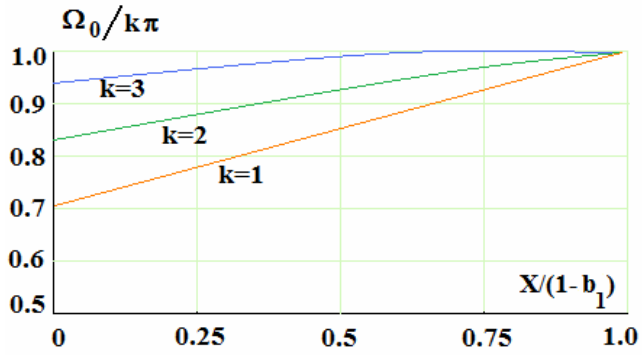

Fig. 5. Normalized pulsation ratio to kπ vs. non-dimensional thickness ratio to (1-b_1)

We present for evidencing one of our many applications using the presented method. Our experiments and theoretical evaluation were done taking a non-metalized propellant, based on *ammonium perchlorate* and *polybutadiene* [4], ($c^* = 1490$ m/s , $\bar{u}_b = 1{,}285\ \bar{p}^{0.474}$).

The grain geometry (Fig. 2) is characterized by the following parameters: b_1 = 0,468, b_2 = 2,660, $\alpha = \pi/3$. The grain length of 50 mm has been established so that the frequency of the fundamental longitudinal mode takes values in the vicinity of 10 KHz. Considering the propellant grain geometry of cylindrical tubular shape, we avoided having discontinuities of the grain core cross-section along the motor's length and thus we facilitated the interpretation of the results.

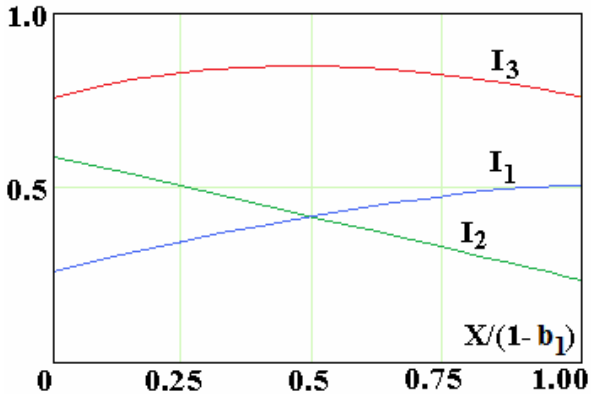

Fig. 6. The integrals I_1, I_2 and I_3 vs. non-dimensional thickness ratio to (1-b_1)

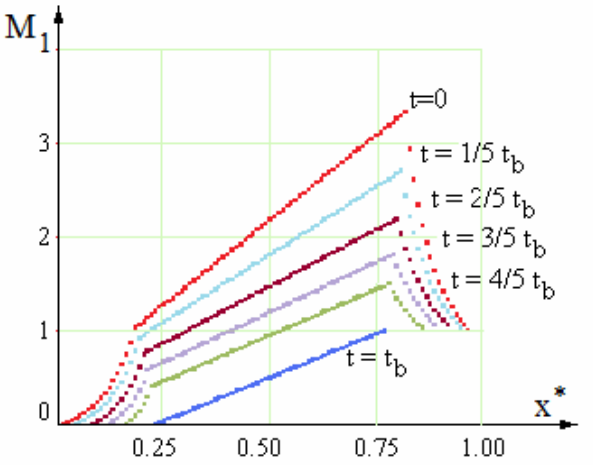

Fig. 7. Mach parameter M_1 vs. non-dimensional length x* at several burning time values

We used the laboratory and presented analytical tools to characterize the acoustic response properties of a solid propellant as a function of frequency for different values of case average pressure.

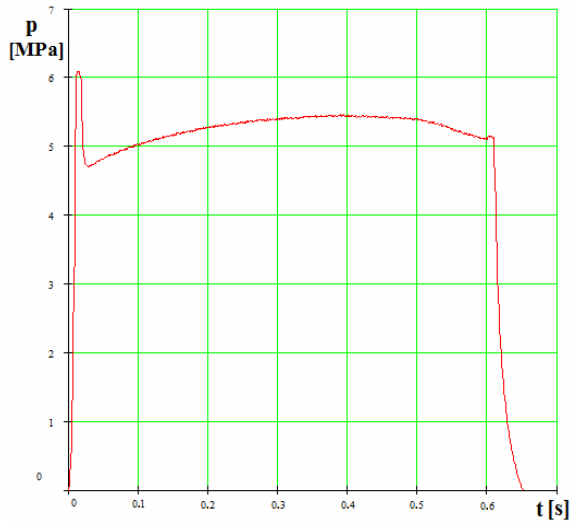

Fig. 8. Experimental head end pressure – time profile, with no disturbances

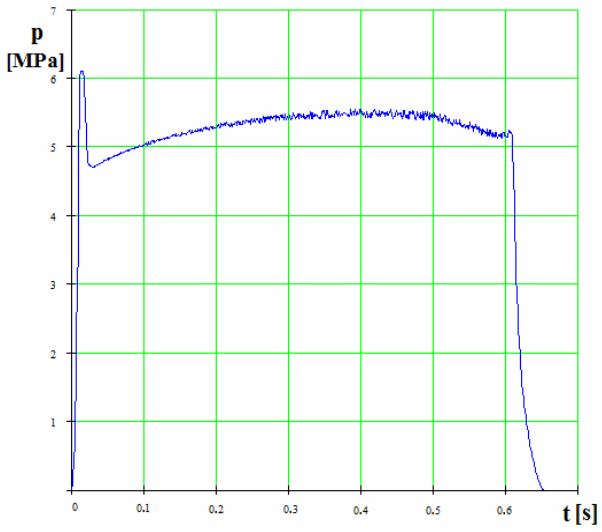

Fig. 9. Experimental head end pressure – time history, with low disturbing intensity

Time evolution of measured chamber pressure using the laboratory setup at low and high disturbing intensity levels (Fig. 9, 10) versus the nominal curve *p(t)* (Fig. 8), basically preserves the average pressure evolution shape. In certain disturbing conditions a perturbed zone can appear (starting from $\approx 0{,}4$ s, Fig. 10) with a significant deviation of the average pressure. This combustion instability phenomenon was pointed out in [4], too.

The variations of frequency and damping parameter (Fig. 11), were computed on the basis of pressure – time records (Fig. 9). These 2 influence factors can be mathematically correlated and they correspond to the same case average pressure. The time – frequency analysis was done for a low level disturbing case and a linear variation of frequency was observed. The real part values of the propellant response, eq. (30) were obtained taking into account the dependence time – damping parameter.

The results concerning the variation of the real part of the propellant response in respect of the frequency is illustrated in Fig. 12. The $R_p^{(r)}$ magnitude is acceptable and we can observe its increasing variation until a maximum value corresponding to a frequency level of about 10 KHz.

An explanation of this variation trend may be found in the unsteady behaviour of the burning zone to high frequency.

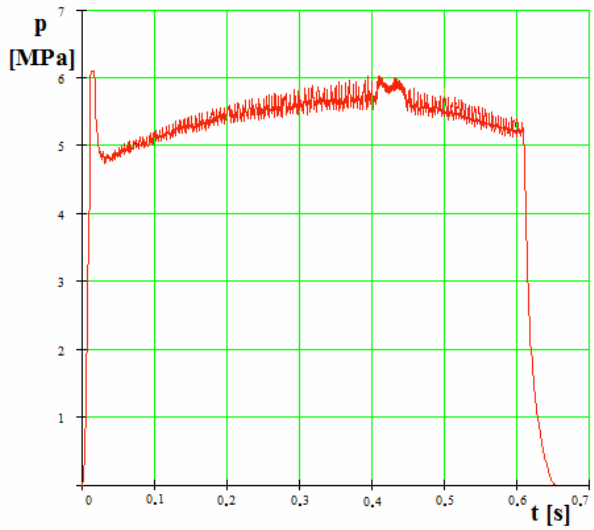

Fig. 10. Experimental head end pressure – time history, with high disturbing intensity

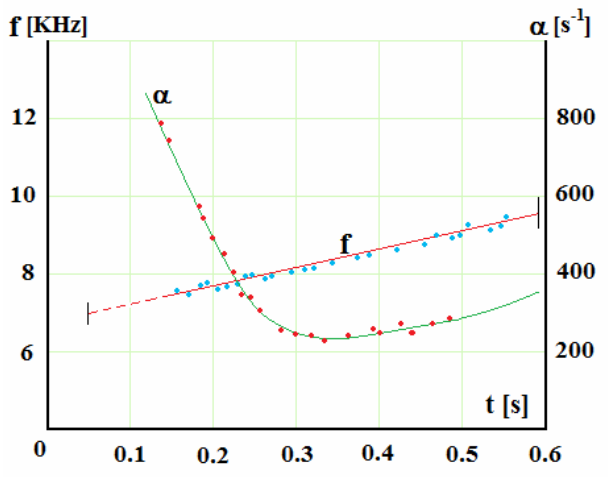

Fig. 11. Frequency and damping parameter of pressure oscillations vs. burning time

The absolute value of $R_p^{(i)}$ doesn't exceed in magnitude some units and it is very sensitive with a_0 (e.g. $-5\%\, a_0$ inducing the response decreasing at about zero) and can influence the average pressure at various frequencies (e.g. – 2 at 7 KHz, –30 at 9 KHz).

Our paper pointed out that during all the tests with the subscale test solid rocket motor, for average pressures of 3-8 MPa, the excited mode was the fundamental longitudinal mode (first and eventual second harmonics).

We have extended the application of the presented model also in the case of a DB propellant [5], (based on NG/NC/DNT, $c^* = 1380$ m/s, $\overline{u}_b = 0{,}675\ \overline{p}^{0.598}$), used for a 122 mm solid rocket motor. Thus, Figure 13 depicts the influence of the mean pressure on the propellant response function, for frequency values of 1-3 KHz. This result is important for a DB propellant rocket motor design, especially with a higher length to diameter grain ratio, and a higher volume charge rate of the motor case.

As an important conclusion for the two case studies, *the most unfavourable propellant response is obtained at smaller pressures,* in the proximity of the stable working limit of the rocket motor. Moreover, the unsteady motor working changes could be accompanied by abrupt rise of average chamber pressure.

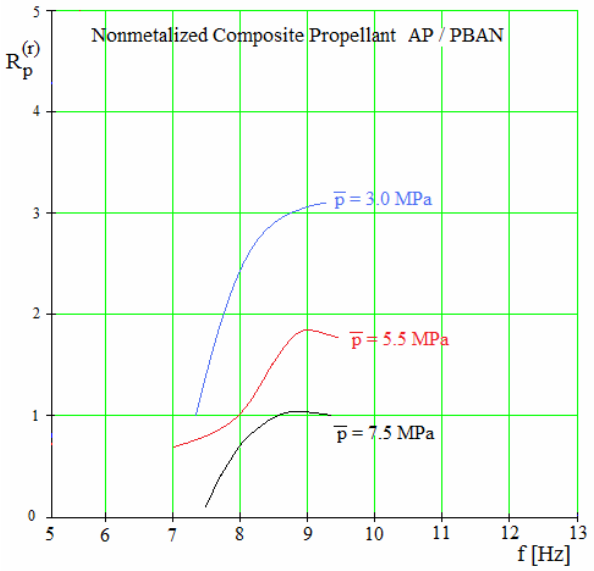

Fig. 12. Real part of coupled pressure response function vs. frequency at 3 case average pressure values – composite propellant

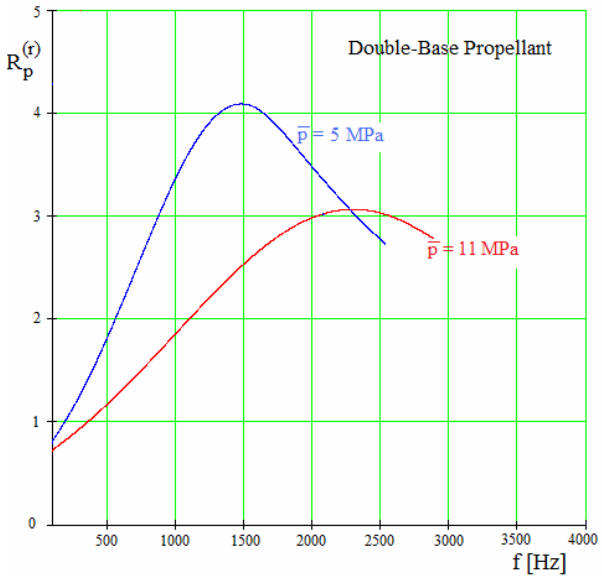

Fig. 13. Real part of coupled pressure response function vs. frequency at 2 case average pressure values – DB propellant

Taking into account the researches made by Kuentzmann and Traineau [3, 4, 6] for several composite propellants we have extended the application of this propellant response evaluation indirect method for the DB propellant mentioned before. Thus, during the tests made with the same solid rocket motor (MR-01, D_R = 122 mm [5]), at two different initial temperatures, we observed that rather high level frequency combustion instabilities can appear in certain conditions and they can induce an important variation of the average pressure evolution (Fig. 14, 15). The most disturbed time-pressure evolution (nonlinear instabilities) was recorded for smaller pressure values, corresponding of negative propellant initial temperature T_i = –40°C (Fig. 15).

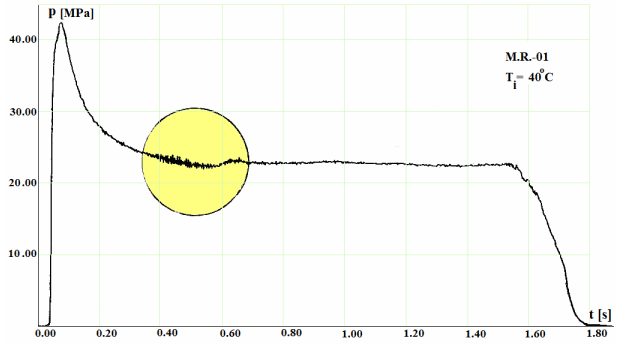

Fig. 14. Pressure/time history, at T_i = 40°C, for DB propellant motor (D_R = 122 mm, [5])

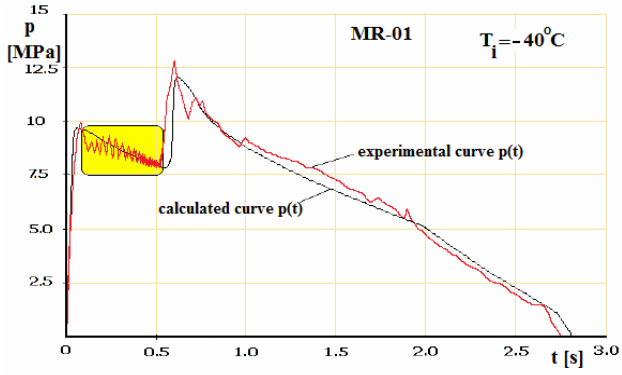

Fig. 15. Pressure/time history, at T_i = –40°C for DB propellant motor (D_R = 122 mm, [5])

This experiment comes to sustain the conclusion concerning the prediction property of propellant response function towards the motor behaviour. Hence, at smaller chamber mean pressures, the high frequency combustion instabilities may have a significant influence on the rocket motor working.

Our linear acoustic analysis can't be applied if the propellant burning rate becomes non-sinusoidal when the pressure oscillation magnitude grows larger than about 10% of the mean pressure [1, 2].

Research towards predicting and quantifying undesirable axial combustion instability symptoms necessitates a comprehensive numerical model for internal ballistic simulation under dynamic flow and combustion conditions. The study model of the present paper, based on perturbations method was included in the mathematical model of a complex simulation computer program of solid rocket motors disturbed operation, which operates with a large thermo-gas-dynamical and engine construction data basis. This is also a benefit of using an indirect evaluation method of coupled pressure propellant response function.

Our next step in the combustion instabilities study will be to carry on the improvement of the mathematical model and to use the jet modulating technique to continue the investigation of DB propellants and to explore the response function of metalized propellants in various operating conditions.

REFERENCES

[1] Blomshield F.S., *Lessons Learned In Solid Rocket Combustion Instability*, American Institute of Aeronautics and Astronautics, Missile Sciences Conference, Monterey, California, November 2006.

[2] Culick F.E.C., Combustion Instabilities in Solid Rocket Motors, *Notes for two lectures of special course "Internal Aerodynamics in Solid Rocket Propellant"*, von Karman Institute, 2002.

[3] Davenas A., *Technologie des Propergoles Solides*, Masson, Paris, 1989.

[4] Kuentzmann P., Laverdant A., *Détermination expérimentale de la réponse d'un propergol solide aux oscillations de pression de haute fréquence*, La recherche aérospatiale, 1984.

[5] Safta D., *Propulsion Thermodynamics and Fly Dynamics Elements*, Military Technical Academy, Bucharest, 2004.

[6] Traineau J.C., Prevost M., Tarrin P., *Experimental low and medium frequency determination of solid propellants pressure-coupled response function*, American Institute of Aeronautics and Astronautics 94-3043, 1994.

[7] Shusser M., Culick F.E.C., Cohen N.S., Combustion response of ammonium perchlorate composite propellants, *Journal of Propulsion and Power*, vol. 18, no. 5, 2002.